Experimental study of unidirectional excitation of SPPs by binary area-coded nanohole arrays

Oubo You (游欧波)[1], Benfeng Bai (白本锋)[1,2*], and Xiaowei Li (李晓炜)[3]

[1] *State Key Laboratory of Precision Measurement Technology and Instruments, Department of Precision Instrument, Tsinghua University, Beijing 100084, China*

[2] *Tsinghua-Foxconn Nanotechnology Research Center, Tsinghua University, Beijing 100084, China*

[3] *School of Mechanical Engineering, Beijing Institute of Technology, Beijing 100081, China*

[*] *Corresponding author: baibenfeng@tsinghua.edu.cn*

Received February 19, 2014; accepted April 29, 2014; posted online July 18, 2014

We present an experimental study on a unidirectional surface plasmon polariton (SPP) launcher based on a compact binary area-coded nanohole array, where the symmetry breaking is realized via effective-index modulation in the binary pattern of the gold film, thus avoiding the challenge of modulating nanostructure in its depth. It is shown that SPPs can be unidirectionally and effectively excited at normal incidence. The SPP intensity and asymmetric excitation ratio, which are two key figure-of-merits of SPP launchers, can be improved by increasing the number of array rows. The proposed device is compatible with most mature top-town nanofabrication techniques and thus is perspective for low-cost mass production.

OCIS codes: 240.0240, 230.0230, 240.6680.

doi: 10.3788/COL201412.082401.

In various plasmonic applications nowadays, such as plasmonic circuitry, unidirectional beaming[1−3], second harmonic generation[4], and sensing[5,6], the efficient excitation and steering of surface plasmon polaritons (SPPs) are of great importance. The SPP launchers are such devices that can couple and convert the energy of free-space propagating light into the SPPs confined on a metal surface. So far, a number of schemes of unidirectional SPP launchers have been proposed[7−26]. Regardless of their different designs and structures, the fundamental principle is to break the symmetry of either the structure or the incident field so that the SPPs can be launched to the desired direction. Typical schemes of breaking the incidence symmetry are, e.g., tuning the oblique incident angle on symmetric subwavelength hole arrays or nanoslits[7−11], switching the polarization state or the helicity of light on a symmetric structure[12−14], or the combination of helicity switching of incident light and an asymmetric structure[15]. If normal incidence is preferred or the polarization state of light cannot be changed, some structures with broken symmetry should be considered, such as double nanoslits with different filling media[16], chirped plasmonic grating[17], depth-varying groove array[18], asymmetric periodic metallo-dielectric multilayers[19], nanocavities with asymmetric geometries[20,21], asymmetric surface corrugation of metal film[22], compact magnetic antennas[23], and slanted surface-relief grating structures[24−26].

In the design of directional SPP launchers, the coupling efficiency of incident light to SPPs, η, and the asymmetric excitation ratio, r (which is defined as the ratio between the SPP intensities launched into the desired direction and the opposite direction), are two key figure-of-merits. Baron *et al.*[18] experimentally realized a SPP launcher with $\eta = 52\%$ and $r = 47$ based on a depth-varying groove array. Since the device was very small (with a length of 8 μm), the coupling efficiency was evaluated only with respect to the portion of light shining on the device area, but not to the full beam. Wang *et al.*[25] proposed an electrically pumped SPP launcher incorporating a slanted grating, which showed a relatively high launching efficiency and an experimental r of about 10. However, these works required careful control of either the groove depth variation to nanometer precision[18] or the tilting angle of the ridges of a slanted grating[25], which imposed much difficulty to nanofabrication and mass production. We have also proposed an r-tunable directional SPP launcher based on a compact double-nanoslit structure previously[11], whose r can be as high as 90 in simulation and 68 in experiment. However, the fine tuning of the incident angle is required for this device, which is not convenient in some applications. Therefore, the binary-structured SPP launchers working under normal incidence would be desired, as they are more compatible with mature nanofabrication techniques such as electron beam lithography (EBL), focused ion beam (FIB) milling, and nanoimprinting lithography (NIL).

Based on these considerations, we have proposed a directional SPP launcher based on a binary area-coded nanohole array (BAHA), as shown in Fig. 1. That is, a metal film that can support propagating SPP mode is perforated with a triangular hole array without any modulation in the z direction (which is thus a "binary" pattern) and the local filling factor of the grating is varied with respect to the spatial coordinate (which thus means "area-coded"). For more details on the binary area-coded grating, the readers may refer to Refs. [26, 27]. This structure realizes symmetry breaking via effective-index modulation in the pattern, thus avoiding the depth control in nanostructures[27]. We have carried out a theoretical study on the design and optimization of the BAHA launcher[26]. However, in the experimental study in that work, the array covered the

whole sample so that we actually characterized the SPP excitation on an infinitely periodic surface plasmon polaritonic crystal[28], but not by the launcher. Therefore, the observed r was only around 1.8, much lower than the theoretical prediction[26]. Here, we perform a systematic experimental study on the unidirectional SPP excitation by the finite-sized BAHA launchers by applying a new experimental scheme, so as to verify the theoretical prediction in Ref. [26]. Furthermore, the dependence of r and excitation efficiency on the number of rows of the array is thoroughly studied in this work, which is important for the practical application of the device.

The device is schematically shown in Fig. 1(a) and is numerically designed according to the method presented in Ref. [26]. The working principle of the device has been detailed in Ref. [26], which realizes unidirectional excitation of SPPs by matching the wave vector of the SPP mode to that of a specific blazed evanescent diffraction order of the grating. A silica substrate is coated with a 10-nm-thick Ti adhesion layer and then a 90-nm-thick gold film (which is thick enough to prevent the directly transmitted light through the film). The metallic films are perforated by an array of isosceles triangle holes with height d and width w. The holes are closely connected with each other so that the grating periods in x and y directions are also w and d, respectively. Since the symmetry breaking is realized via the effective-index modulation in y direction, the array is designed to be infinitely periodic in x direction. In y direction, we keep the number of rows N as a variable so as to investigate the dependence of r on N. For the convenience of experimental characterization, the device is back illuminated by a y-polarized (named TM hereafter) plane wave at a wavelength of 1064 nm. The SPPs are excited on the top surface and propagate in the $\pm y$ directions.

The SPP excitation in the BAHA device was rigorously simulated by a commercial software package COMSOL 4.3 based on the finite element method. The refractive

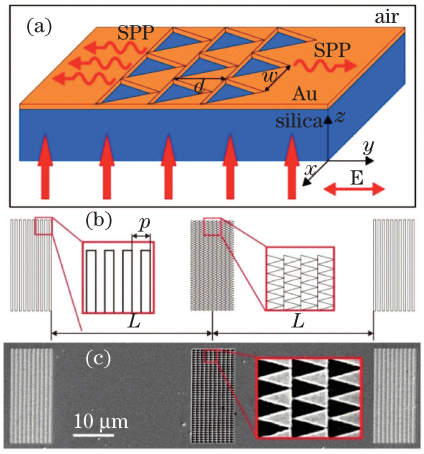

Fig. 1. (a) Schematic of the BAHA-based unidirectional SPP launcher, which is back illuminated by a 1064 nm laser. SPPs are excited on the air-gold surface and propagate in $\pm y$ directions asymmetrically. (b) Layout of an experiment sample consisting of a BAHA launcher in the central area and two decoupling groove arrays at the left and right sides. (c) SEM image of a fabricated sample with 10 rows of triangular holes in the BAHA area.

indices of silica and gold were taken as 1.4496 and 0.2698 + 7.1712i, respectively. Since the BAHA excites SPPs via its (0, ±1)th diffraction orders, the period d is optimized as 1057 nm by following the design process in Ref. [26] and the triangle hole width w (which should be much smaller than d) is taken as 570 nm ($\sim d/2$). To detect the SPP excitation by a far-field imaging method[11], two shallow groove arrays were etched symmetrically at the left and right sides of the BAHA with $L = 40$ μm, acting as the decoupling gratings to convert the received SPPs to radiative light, as shown in Fig. 1(b). The period of the decoupling groove arrays was chosen as $p = \lambda_{SPP} \approx 1053$ nm, the duty cycle was 0.5, and the groove depth was 60 nm. In numerical simulation, we set a calculation area of 110-μm long in y direction (to include both the BAHA area and the two decoupling groove arrays) and 0.57-μm wide in x direction (with the periodic boundary condition applied).

We simulated the SPP excitation by the BAHA launchers with different rows of triangular holes. To take into account the practical experimental condition as much as possible, the incident light is treated as a Gaussian beam with a beam waist radius of 25 μm so that it does not cover the decoupling groove arrays. Figure 2 shows the calculated distribution of the electric field amplitude $|\mathbf{E}|$ on the top surface of a BAHA with 10 rows of triangular holes. The $|\mathbf{E}|$ value was normalized to the incident field amplitude. It is evident in Fig. 2(a) that under TM-polarized illumination, a confined field is excited on the upper surface of the BAHA and propagates mainly toward the left side (i.e., the -y direction). In contrast, under x-polarized (named TE) incidence, no such confined field is excited (not shown here), verifying the SPP excitation only by TM illumination. In Fig. 2(b), we show the field distributions on the surface of the whole sample that is 110-μm long in y direction, by comparing two cases with and without the decoupling groove arrays. It is seen that by inserting the decoupling grooves the field intensity and distribution in the original system are not disturbed too much; the only change is the fluctuation of field in the regions between the BAHA and the decoupling groove arrays, owing to the formation of SPP standing waves caused by the interference of the forward and backward propagating SPPs in these regions. To evaluate the SPP asymmetric excitation ratio r, we took the field power flows at two symmetric positions of $y = \pm 20$ μm and got their ratio. The derived r is 13.7 and 15 for the cases with and without the decoupling grooves, respectively. These simulation results show that the characterization of SPP excitation intensity by inserting the decoupling groove arrays is feasible, although r may deviate a bit.

It is also found in simulation that the vertex sharpness of the triangular hole may affect the derived r significantly. For example, when the radius increases from 4 to 24 nm in a simulation example, r may decrease from about 12 to 7.5. Hence, by taking into account the practical FIB fabrication process of the sample in which the ion beam diameter is about 40 nm, we took the vertex radius of triangular holes as 20 nm in all our simulations.

Based on the above theoretical analysis, we carried out experiments to investigate the asymmetrical SPP

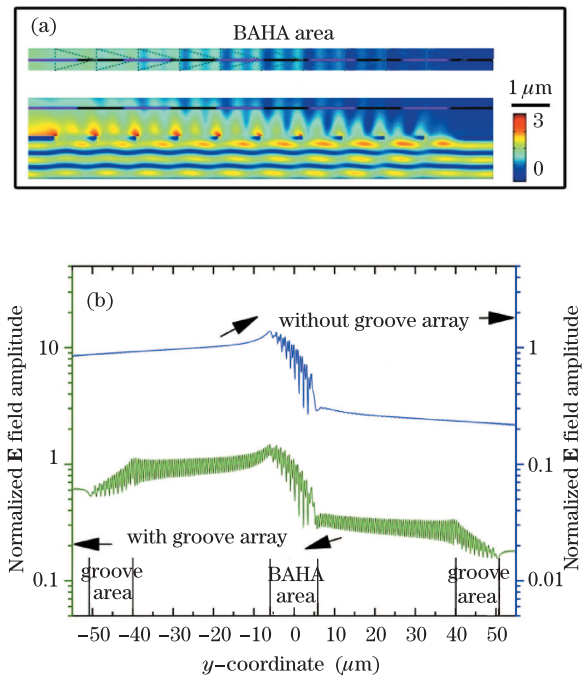

Fig. 2. (a) Simulated $|\mathbf{E}|$ distribution on the air-gold surface of a BAHA with 10 rows of triangular holes and without the decoupling groove arrays. Top: field distribution in the xy plane. Bottom: field distribution in the yz cross-section plane. The color scale is in the unit of the incident field amplitude. (b) $|\mathbf{E}|$ distribution on the BAHA surface along the dashed line indicated in (a). The upper and lower curves correspond to the results with and without the decoupling groove arrays, respectively. The vertical axes are in the unit of the incident field amplitude.

excitation in the BAHAs. We have fabricated 10 samples of BAHAs with the number of rows N varying from 1 to 10 by FIB milling with a FEI Nova 200 Nanolab system. In each BAHA, 40 triangular holes were etched in each row in the x direction to represent an infinitely periodic array, while the number of rows N was varied. Figure 1(c) shows the scanning electronic microscope (SEM) image of a fabricated sample consisting of a 10-row BAHA and two decoupling groove arrays. A far-field microscopic imaging setup was employed to characterize the SPP excitation, as shown in Fig. 3(a). A linearly polarized laser beam was first transformed into circularly polarized light by a quarter-wave plate (QWP). Then a linear polarizer (LP) was used to generate TE or TM polarized light with the same intensity. At back incidence, some of the incident light penetrated through the triangular holes and excited SPPs on the air-gold interface, which propagated toward the $\pm y$ directions and arrived at the two decoupling groove arrays. Then the two groove arrays converted the SPPs to radiative light propagating away from the film, and the radiative light was collected by a long-working-distance objective (Ob) (Nikon, 40×, NA=0.60) and imaged onto a charge coupled device (CCD). The incident light was attenuated to ensure that the detected CCD signal was not saturated. Then the detected signal intensity on the groove area can be regarded to be proportional to the received SPP intensity.

The detected CCD images of a 5-row and a 9-row BAHA samples under TE- and TM-polarized illuminations are presented in Figs. 3(b)−(e). In the field of view of the CCD, up to three bright speckles can be observed. The central one is the directly transmitted light from the BAHA area, while the left and right hard to distinguish speckles are caused by the radiated light converted by the decoupling groove arrays from the received SPPs. To evaluate the intensity of SPPs and the asymmetric excitation ratio r, the CCD pixel grey values in the region of each decoupling groove area were integrated. Note that since the right speckle was too weak to be distinguished from the dark background, we just integrated the intensities in a region symmetric to the left one about the central bright speckle.

Figure 4 summarizes the theoretical and experimental results of the ten BAHA samples with the number of rows from 1 to 10. To facilitate comparison, all the experimental and simulation results are normalized with the measured and simulated intensities of the left speckle of the 10-row sample, respectively. It means that the theoretical and experiment intensities of the left speckle of the 10-row sample are both 1 (in arbitrary units). It is

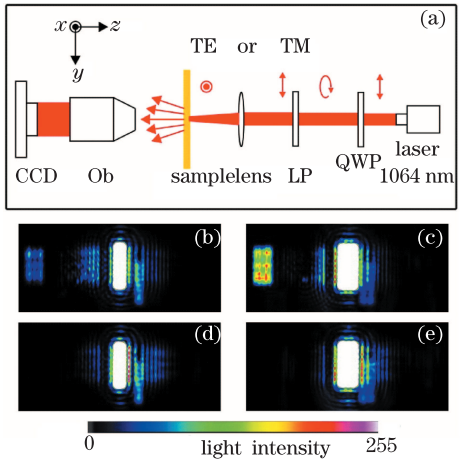

Fig. 3. (a) Schematic of the far-field microscopic imaging setup for characterizing the SPP excitation in the BAHAs. (b) and (c) are the detected CCD images (false color image) of a 5-row and a 9-row BAHA samples under TM illumination, respectively. (d) and (e) are similar to (b) and (c), but under TE illumination.

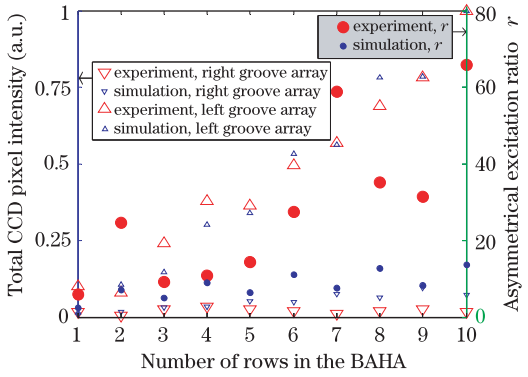

Fig. 4. Comparison of the simulated and experimentally measured light intensities emitted from the left and right decoupling groove arrays as well as the derived asymmetrical excitation ratio r in ten BAHA samples with the number of rows varying from 1 to 10.

seen in Fig. 4 that the theoretical and experimental results correspond to each other relatively well, especially by viewing their trends with respect to the change of the number of rows. It clearly demonstrates the following important facts:

(1) Unidirectional excitation of SPPs can be effectively realized by this compact, single-layered, binary-structured BAHA at normal incidence.

(2) The intensity of the unidirectionally excited SPPs (to the left side) increases almost linearly with respect to the increase of N, while keeping the SPP intensity excited to the opposite direction (the right side) almost unchanged.

(3) The asymmetric excitation ratio r also increases with respect to the increase of N. As can be estimated from Fig. 4, the r derived from the numerical and experimental data are from 2.5 to 13.7 and from 6 to 65.8, respectively, with the increase of N from 1 to 10. However, we should emphasize that this estimation is not accurate and cannot act as a quantitative evaluation of r. Since the right side speckle is very weak (whose signal intensity is even in the background noise level of the CCD), many factors may affect its absolute value markedly, such as the fluctuation of the environment temperature and the laser beam intensity, the slight shift of the inhomogeneous light spot, and the alignment error in the characterization setup. Therefore, even a small error in the detected intensity value of the dark speckle may lead to a remarkable change of r. For this reason, we cannot make an accurate quantitative comparison between the theoretical and experimental r.

The above analyses indicate that in principle one can increase the excited SPP intensity and the asymmetric excitation ratio r just by increasing N. However, in practice, the device size is often restricted by many factors such as other components integrated with the launcher. Therefore, N cannot be very large. But one can always try to maximize it by matching the grating area with the illuminating spot size.

In conclusion, we carry out an experimental study on the unidirectional SPP excitation by a compact, single-layered, binary-structured launcher. The device realizes symmetry breaking by effective-index modulation in an area-coded binary structure, thus avoiding modulating nanostructure in its depth. Experimental results evidently show the unidirectional excitation of SPPs at normal incidence, which coincide with the numerical simulation well. By studying the samples with different numbers of triangular hole arrays N, it is demonstrated that the excited SPP intensity as well as the asymmetric excitation ratio can be effectively improved by increasing N, if the device size can meet the incident beam size and the integration requirement. The BAHA-based unidirectional SPP launcher can be designed with reasonable geometric parameters so that it can be fabricated by most mature nanofabrication techniques such as EBL, FIB, and NIL, and thus is perspective for low-cost mass production.

This work was supported by the National Natural Science Foundation of China (No. 61227014) and the Ministry of Science and Technology of China (No. 2011BAK15B03).

References

1. H. Kim, J. Park, and B. Lee, Opt. Express **34,** 2569 (2009).
2. Y.-L. Hua and Z.-Y. Li, J. Appl. Phys. **105,** 013104 (2009).
3. X. Li, Q. Tan, B. Bai, and G. Jin, Chin. Opt. Lett. **10,** 052401 (2012).
4. H. Yin, Y. Liu, Z. Yu, Q. Shi, H. Gong, X. Wu, and X. Song, Chin. Opt. Lett. **11,** 101901 (2013).
5. R. D. Roy, R.Chattopadhyay, and S. K. Bhadra, Photon. Res. **1,** 164 (2013).
6. M. Chamanzar, Z. Xia, S. Yegnanarayanan, and A. Adibi, Opt. Express **21,** 32086 (2013).
7. J.-Y. Laluet, E. Devaux, C. Genet, T. W. Ebbesen, J.-C. Weeber, and A. Dereux, Opt. Express **15,** 3488 (2007).
8. H. Kim and B. Lee, Plasmonics **4,** 153 (2009).
9. Z. Wang, M. Zhang, J. Wang, F. Lu, K. Li, and A. Xu, Appl. Phys. Lett. **101,** 061107 (2012).
10. I. P. Radko, S. I. Bozhevolnyi, G. Brucoli, L. Martín-Moreno, F. J. García-Vidal, and A. Boltasseva, Opt. Express **17,** 7228 (2009).
11. X. Li, Q. Tan, B. Bai, and G. Jin, Appl. Phys. Lett. **98,** 251109 (2011).
12. S.-Y. Lee, I.-M. Lee, J. Park, S. Oh, W. Lee, K.-Y. Kim, and B. Lee, Phys. Rev. Lett. **108,** 213907 (2012).
13. L. Huang, X. Chen, B. Bai, Q. Tan, G. Jin, T. Zentgraf, and S. Zhang, Light Sci. Appl. **2,** e70 (2013).
14. F. J. Rodríguez-Fortuño, G. Marino, P. Ginzburg, D. O'Connor, A. Martínez, G. A. Wurtz, and A. V. Zayats, Science **340,** 328 (2013).
15. J. Lin, J. P. B. Mueller, Q. Wang, G. Yuan, N. Antoniou, X.-C. Yuan, and F. Capasso, Science **340,** 331 (2013).
16. T. Xu, Y. Zhao, D. Gan, C. Wang, C. Du, and X. Luo, Appl. Phys. Lett. **92,** 101501 (2008).
17. J.-S Bouillard, S. Vilain, W. Dickson, G. A. Wurtz, and A. V. Zayats, Sci. Rep. **2,** 829 (2012).
18. A. Baron, E. Devaux, J.-C. Rodier, J.-P. Hugonin, E. Rousseau, C. Genet, T. W. Ebbesen, and P. Lalanne, Nano. Lett. **11,** 4207 (2011).
19. A. Roszkiewicz and W. Nasalski, Proc. SPIE **8424,** 842426 (2012).
20. J. Chen, Z. Li, S. Yue, and Q. Gong, Appl. Phys. Lett. **97,** 041113 (2010).
21. G. Lerosey, D. F. P. Pile, P. Matheu, G. Bartal, and X. Zhang, Nano. Lett. **9,** 327 (2009).
22. F. López-Tejeira, S. G. Rodrigo, L. Martín-Moreno, F. J. García-Vidal, E. Devaux, J. Dintinger, T. W. Ebbesen, J. R. Krenn, I. P. Radko, S. I. Bozhevolnyi, M. U. González, J. C. Weeber, and A. Dereux, New J. Phys. **10,** 033035 (2008).
23. Y. Liu, S. Palomba, Y. Park, T. Zentgraf, X. Yin, and X. Zhang, Nano. Lett. **12,** 4853 (2012).
24. N. Bonod, E. Popov, L. Li, and B. Chernov, Opt. Express **15,** 11427 (2007).
25. L. Wang, T. Li, L. Li, W. Xia, X. G. Xu, and S. N. Zhu, Opt. Express **20,** 8710 (2012).
26. B. Bai, X. Meng, J. Laukkanen, T. Sfez, L. Yu, W. Nakagawa, H. P. Herzig, L. Li, and J. Turunen, Phys. Rev. B **80,** 035407 (2009).
27. B. H. Kleemann, J. Ruoff, and R. Arnold, Opt. Lett. **30,** 1617 (2005).
28. A. V. Zayats and I. I. Smolyaninov, J. Opt. A Pure Appl. Opt. **5,** S1 (2003).